The Astronomical Journal, 136:1857–1865, 2008 November doi:10.1088/0004-6256/136/5/1857

ORBIT-RESOLVED PHOTOMETRY AND ECHELLE SPECTROSCOPY OF THE CATACLYSMIC VARIABLE ST LMi DURING A 2007 HIGH STATE

Jeff W. Robertson[1], Steve B. Howell[2], R. K. Honeycutt[3], S. Kafka[4], and T. Campbell[5]
[1] Department of Physical Sciences, Arkansas Tech University, Russellville, AR 72801-2222, USA; jrobertson@atu.edu
[2] NOAO/Kitt Peak National Observatory, Tucson, AZ 85719, USA; howell@noao.edu
[3] Department of Astronomy, Indiana University, Bloomington, IN 47405, USA; honey@astro.indiana.edu
[4] *Spitzer* Science Center, California Institute of Technology, Pasadena, CA 91125, USA; stella@caltech.edu
[5] Whispering Pines Observatory, Harrison, AR 72601, USA; jmontecamp@yahoo.com
Received 2008 April 28; accepted 2008 August 22; published 2008 September 30

ABSTRACT

We present high-resolution echelle spectra and contemporaneous photometry of the polar ST LMi during a high state in 2007 March. Emission lines at Hα, He I λ5876, and He I λ7065 show similar line profiles over orbital phase and have narrow and broad components. These profile changes with phase are very similar to those reported in earlier high-state studies of ST LMi. The radial velocity curves from double Gaussian fits to the line profiles are interpreted as two crossing curves, neither of which is coincident with the orbital motion of the secondary star. We attribute one component to infall motions near the white dwarf and the other to a gas streaming along magnetic field lines connecting the two stars.

Key words: binaries: close – novae, cataclysmic variables – stars: individual (ST LMi)

Online-only material: color figures

1. INTRODUCTION

Cataclysmic variables (CVs) are short-orbital-period interacting binaries with a white dwarf (WD) primary star accreting hydrogen-rich material from a late-type mass-losing secondary dwarf star. Angular momentum loss over evolutionary timescales in the system decreases the orbital period and shrinks the Roche Lobe, allowing material to siphon from the secondary star, through the inner Lagrangian point (L1), and fall toward the WD. In systems where the WD magnetic field is strong enough ($\gtrsim 10^7$ G), called polars, material from the secondary free-falls from the L1 point between the two stars toward the WD until disrupted by the strong magnetic field of the WD at the coupling region. It is then channeled down along magnetic field lines toward one or both poles of the WD. A shock near the surface of the WD slows the material and generates short-wavelength radiation. When the magnetic field of the WD is lower, as in nonmagnetic CVs, the L1 overflow material forms an accretion disk around the WD that then provides most of the light in the visible, as well as much of the dynamics for variability that make CVs famous. A review of CVs and their properties can be found in Warner (1995) and Hellier (2001).

We obtained simultaneous photometry and echelle spectroscopy of the polar ST LMi during a high state in 2007 March. This gives us the opportunity to study in detail what is considered to be a one-pole accretor in its high state. ST LMi has been considered throughout its history to be the textbook example of a polar whose main accretion region is self-eclipsed by the WD, allowing extraction of the geometry of the accreting regions. A nice review of the derived system parameters by various investigators is presented by Potter (2000): system inclination between 56° and 69°, magnetic dipole offset between 33° and 56°, and magnetic field strength of the main accreting pole between 11.5 and 30 MG. Furthermore, a complex, arc-like emitting region was derived in the near-infrared (near-IR) spectra by Ferrario et al. (1993).

Although ST LMi is treated as primarily a one-pole accretor (Stockman et al. 1983; Cropper 1986; Stockman & Schmidt 1996), a second accreting region has been revealed by a positive circular polarization in the near-IR (*H* and *J* bands) located at phase ~0.35. (Peacock et al. 1992). Near this same phase, Bailey et al. (1985) reported a second "hump" in their IR *J*, *H*, *K* photometry, which they interpret as emission on or near the secondary star. Their Stokes imaging revealed a low-temperature, low-density, main magnetic pole, responsible for the majority of the observed emission lines, followed by a secondary high-density, high-temperature emission region closer to the secondary pole (Potter 2000). Also, Bailey et al. (1985) noted a small difference in the duration of the photometric maximum during two years of their observations (1982 and 1983). They argue that this cannot be the result of height increase of the emitting shock region, and they conclude that there should be a small precession of the main dipole axis. Such a behavior was not observed in long-term light curve RoboScope data (Kafka et al. 2007); however, the sampling rate of that data set would not allow for the study of small temporal changes in the system's geometry.

In 2007, we presented a spectroscopic and photometric study of the low state of this system during 2005–2006 discussing magnetic activity on the lower-mass, ultra-fast rotating secondary star (Kafka et al. 2007). The results of that study indicate that during its low state, ST LMi has an occasional hump in the optical light curve between phases 0.5 and 0.95 even while faint at around *V* 17.5 mag. This is the same phase interval during which the "bright" phase in the high state occurs due to the high visibility of the accretion pole. Therefore, episodic low-level accretion is suspected to take place even during the low state. The low-state spectra of ST LMi are dominated by TiO bands from the secondary star with the only emission coming from the Hα line. The emission profiles are similar to AM Her and VV Pup during their low states. Concurrent photometry and spectroscopy of ST LMi in the low state supports a lack of much accretion and a cool dark starspot region near the L1 point.

Table 1
Photometric Targets

ID	α_{2000}	δ_{2000}	V	$B-V$
ST LMi	11:05:39.75	+25:06:28.9	15.0[a]	
HH95-2 C	11:05:43.28	+25:08:59.3	15.124	0.574
HH95-5 K	11:05:28.70	+25:10:43.7	16.347	0.901

Note. [a] ST LMi V magnitude is high state, "out-of-hump" phase brightness (e.g., WD accreting pole not in view).

The system also showed a drop in brightness 0.7 mag fainter than its low-state level which could be an indication of complete cessation of accretion or some other change in the system.

That same study suggested that such activity signatures are also likely to be present during the high state. Moderate-resolution spectra during the high state of the system that showed variable and complex emission line profiles at Hα were also included.

The new spectroscopic data reported in this paper have significantly improved spectral resolution, promising to better delineate the complex emission regions in this system using Gaussian decomposition of the components of the line profiles. We also obtained orbit-resolved photometry of ST LMi that is simultaneous with the spectroscopy, helping complete our description of the ST LMi high state at this epoch. In the following sections, we describe the observations (Section 2) and analysis (Section 3), followed by discussion of the results in Section 4.

2. OBSERVATIONS

2.1. Photometry

ST LMi was observed photometrically during UT 2007 March 8 and 9, the latter date being simultaneous with echelle spectroscopy. The observations were made at a dark site in the Arkansas Ozarks with a 0.3 m, $f/10$ Schmidt–Cassegrain with an $f/6.3$ focal reducer and an SBIG ST-9E CCD camera unfiltered. The camera was thermo-electrically cooled to -10 °C. A $15' \times 15'$ portion of the ST LMi field was observed over several hours each night with exposure times of 90 s.

All of the CCD images were processed using `Cmuniwin`,[6] a PC(WIN)-based software developed from Linux FORTRAN and C programs originally developed by Filip Hroch (1998). In short, the images are converted to FITS, if necessary, dark-subtracted and flat-fielded if desired, processed to find stellar targets, and photometrically measured utilizing the algorithms of DAOPHOT (Stetson 1987). The target lists are pattern-matched against each other to identify identical stars in each image via the algorithm of Groth (1986), and variable, comparison, and check stars are selected to generate differential light curves with the option of doing incomplete ensemble photometry (Honeycutt, 1992) to search for variables.

Details of the comparison and check stars taken from Henden & Honeycutt (1997) used for differential photometry are found in Table 1. The standard deviations of the magnitude differences between the comparison and check stars on each night were 0.06 and 0.07 mag, respectively, giving an indication of the reliability of the photometry. Differential extinction was reduced by selecting comparison stars of similar color to each other and to the variable.

[6] http://c-munipack.sourceforge.net/

2.2. Spectroscopy

Echelle spectra were obtained at the Kitt Peak National Observatory 4 m Mayall telescope on UT 2007 March 9. The echelle spectrograph was used with the T1KA CCD and a GG495 filter employing a cross-dispersed setup of 31.6 lines mm^{-1} and a blaze angle of 63.°4. This setup and a 1.″5 slit yielded a 2 pixel resolution of 0.16 Å. The two-dimensional CCD received echelle orders 77–97 covering 5750–7245 Å. The seeing varied from 1.0 to 1.″2 throughout the night and observations of spectrophotometric standards, as well as visual inspection of the guide star indicated a photometric night. ST LMi was observed for approximately 4 hr with exposure times of 600 s. Th–Ar comparison lamps were obtained before, after, and during each of the time series runs. The continuum level was not reached due to the high dispersion and short integration times used. This was not a detriment in our observations as our motivation was to look for rapid changes in the hydrogen and helium emission lines, especially the profile of Hα. Times and measurements of the individual spectra are found in Table 2.

Standard IRAF[7] tasks were used to process the frames into one-dimensional spectra using the `noao.imred.echelle` package. The spectra were first processed to remove instrumental/detector artifacts (i.e., bad columns, bias, flat-field, cosmic rays) and then `apall` was used to define the apertures for each echelle spectral order on the chip from an object image constructed from a median of all the individual object spectra. A total of 22 orders were extracted from all 29 individual object spectra corresponding to spectral coverage from 5750 Å to 7900 Å. No sky subtraction or extinction correction was applied. Wavelength calibration was done for each spectral order of interest with the Th–Ar calibration lamp images using `ident`, `reident`, `refspec`, and `dispcor`. The spectra were then converted to the heliocentric frame of reference with `rvcor` and `dopcor`. Spectral orders of interest included numbers 2, 12, 14, and 18 corresponding to the emission lines He I λ5875, Hα λ6563, He I λ6678, and He I λ7065. The rest of the spectral orders were featureless. Additionally, echelle order 18 had considerably less signal-to-noise ratio (S/N) than the others and the order containing He I λ6678 found the line at the edge of the echelle order so it was truncated in most of the exposures.

3. ANALYSIS

The unfiltered differential photometry of ST LMi on UT 2007 March 8 and 9 is shown in Figure 1. Lines in the bottom panel of Figure 1 on UT 2007 March 9 mark the midexposure times of our contemporaneous spectral observations indicating very good sampling over all orbital phases during this high state. Using an orbital ephemeris HJD 2450596.9006 + 0.07908908 × n, adopted by Kafka et al. (2007), orbital phased light curves for the same two nights are shown in Figure 2. Phase zero corresponds to inferior conjunction of the secondary star. A roughly flat light curve exists for phases outside of 0.55–0.90 when the main accretion pole is being self-eclipsed by the WD. This is contrasted with a gradual brightening and quicker fading during those phases. This behavior resembles the ST LMi high-state light curves of Cropper (1986) and is characteristic for

[7] IRAF is distributed by the National Optical Astronomy Observatories, which are operated by the Association of Universities for Research in Astronomy, Inc., under cooperative agreement with the National Science Foundation.

Table 2
Spectroscopic Observations of ST LMi UT 2007 March 9

HJD−2,454,168	Orbital Phase	$V_R A$	$V_R B$	FWHM$_A$	FWHM$_B$
0.6700154	0.347	−182.4	95.64	24.14	7.5
0.6775268	0.442	−334.8	−13.7	16.1	8.8
0.6850729	0.538	−91.4	−217.6	43.9	18.4
0.6925017	0.632	327.3	−190.4	32.2	13.8
0.6999248	0.726	652.7	−8.0	23.5	22.5
0.7073600	0.820	595.1	90.1	20.8	18.7
0.7147950	0.914	565.6	225.3	11.3	18.2
0.7222190	0.007	195.0	460.4	24.3	8.9
0.7341999	0.159	3.4	247.0	30.4	9.3
0.7417149	0.254	−119.6	156.2	25.2	9.8
0.7491400	0.348	−187.6	122.2	22.0	6.1
0.7565720	0.442	−316.1	−5.5	16.5	8.9
0.7640005	0.536	−102.2	−223.8	36.7	17.5
0.7792376	0.728	613.6	−44.5	27.5	22.3
0.7898139	0.862	578.9	184.6	16.6	21.6
0.7972457	0.956	522.3	219.6	10.2	21.4
0.8046701	0.050	162.0	411.5	24.1	10.1
0.8121024	0.144	−0.8	258.0	30.8	9.5
0.8198103	0.241	−98.7	164.7	23.4	9.7
0.8272409	0.335	−171.5	119.6	21.8	7.4
0.8390150	0.484	−369.8	−71.6	14.4	13.0
0.8464484	0.578	329.5	−216.5	23.1	17.3
0.8538647	0.672	512.3	−128.9	29.2	18.4
0.8612896	0.766	617.3	32.0	22.9	21.7
0.8687219	0.860	602.9	233.8	15.9	20.6
0.8761589	0.954	532.5	226.1	9.1	21.5
0.8865866	0.086	26.05	337.1	27.5	15.3
0.8940102	0.180	−47.4	237.9	28.0	9.5
0.9014415	0.274	−93.7	170.4	21.0	8.7

magnetic accretion onto a single pole. The bright "hump" in the light curve corresponds to the main accretion pole being most nearly along the line of sight to the observer. The peak in the light curve appears near phase 0.78 while there is a sharp drop near phase 0.87. This drop in light likely signals the disappearance of the accretion pole over the WD limb.

The spectra of the echelle order containing the Hα λ6563 line are shown in Figure 3 sorted by orbital phase. The profile of the Hα line changes dramatically over the orbital cycle. The spectra of the echelle order containing the He I λ5876 line are shown in Figure 4, also sorted by phase. The profile of the He I line mimics the profiles found at Hα. The spectra of the echelle order containing the He I λ7065 line are shown in Figure 5. Each of the lines behaves very similarly to one another in their profiles at the same orbital phase. Their profiles are also consistent with those seen by other observers (Stockman et al. 1983; Bailey et al. 1985; Kafka et al. 2007), albeit at a higher spectral resolution in our case.

Comparing our echelle spectra taken during adjacent orbits of the system, we find that there is some variation in line profiles at the same phase (see, for example, the two spectra at orbital phases 0.44 and 0.54). This variability is not surprising considering the magnetic accretion processes happening in this system during the high state.

These echelle spectra suggest two components with varying radial velocity (RV) and widths that create the line profiles at each orbital phase. Fits to the spectral line profiles in Figures 3 and 4 were accomplished with a double Gaussian fit. The IRAF:splot deblend routine and as a check, a commercial program (ORIGINPRO) utilizing a double Gaussian fitting algorithm were employed, both yielding the same results.

Table 3
ST LMi Component γ Velocities from RV Fits

Wavelength	γ_A (km s^{-1})[a]	K_A (km s^{-1})[a]	γ_B (km s^{-1})	K_B (km s^{-1})
Hα (6563 Å)	+164 ± 17	459 ± 22	+100 ± 9	250 ± 12
He I (5876 Å)	+333 ± 18	498 ± 24	+249 ± 11	293 ± 15
Brγ (2.16 μm)	+51 ± 5	+279 ± 7		
Na-I (2.21 μm)[b]	+79.7 ± 41.7	407.5 ± 48		

Notes.
[a] Component A, while fitted with a sine curve to get K-amplitude and γ, is not very sine-like but a sawtooth shape consistent with an origin in a bent gas stream.
[b] In this case, γ and K_2 of the secondary star.

The double Gaussians are able to reproduce the line profiles extremely well at nearly all phases although there are a few phases that seem to call for additional satellite components (e.g., 0.54, 0.67). Fitted Gaussians for the Hα spectral line at some example phases selected to represent the changing line profile over the entire orbit are shown in Figure 6. The RVs of the two emission components obtained from this double Gaussian fitting for ST LMi are shown in Figure 7 for Hα. Strictly, sine fits to the RVs of Hα and He I (this paper) and Brγ and Na I (S. B. Howell et al. 2008, in preparation) yield γ velocities and K amplitudes for components as listed in Table 3.

4. DISCUSSION

First we wish to compare the high-state spectroscopic results from UT 2006 May 19 (at ∼1.3 Å resolution) reported in Kafka et al. 2007 (Paper I), with the new high-state echelle spectra in this study, acquired UT 2007 March 9 at ∼0.16 Å resolution. By visually comparing the line profiles as a function of phase in Figure 11 of Paper I with those in Figure 3 of this paper, we see that, at the same phases, the profiles are nearly identical. The fact that a ∼8× improvement in spectral resolution revealed little new structure indicates that the major line components are already resolved at ∼1 Å, an important point for observers planning further high-state spectroscopic studies of this system. Equally important, the systematic changes of the high-state line profiles with phase are seen to be stable over the ∼10 month interval separating the two observing runs. Finally, we note that the line profiles are nearly identical for He I and for Hα, at the same phases.

Figure 7 shows the RV curves from the echelle spectra using double Gaussian fits. For comparison we also plot the RVs of the Brγ emission line from lower-resolution IR spectra (S. B. Howell et al. 2008, in preparation) and the best-fit sine curve to the RVs of the IR absorption lines of Na I in the K band (Howell et al. 2000, S. B. Howell et al. 2008, in preparation). These absorption features originate in the photosphere of the secondary star and unambiguously determine the orbital phasing of the secondary star.

Despite the similarities of the emission line profiles from Paper I and these new echelle spectra, the two high-state RV curves (Figure 12 in Paper I and Figure 7 of this paper) do differ. The reason is that the line profiles are complex, often with assymetries and multiple components, making the RV results sensitive to the method of extraction of velocities from the emission line profiles. In Paper I, the RVs of the high-state data were determined both by centroiding of the full line and by using the RV of the individual peaks when the line was double peaked. In this paper, the RVs were determined by using

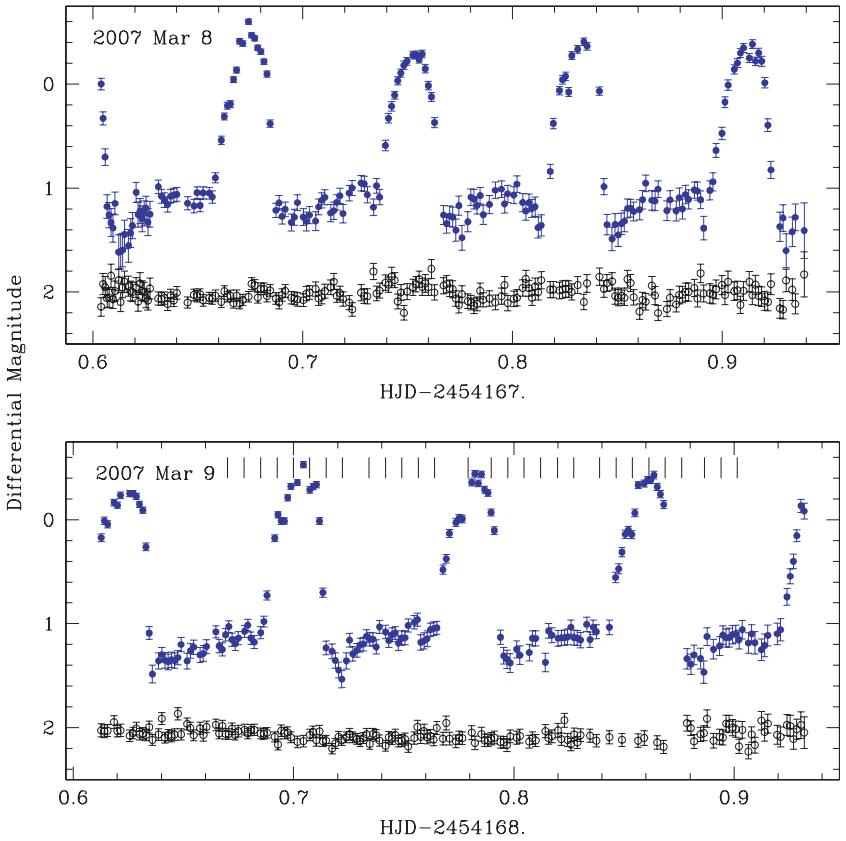

Figure 1. Unfiltered differential photometry of ST LMi during a high state in 2007. The filled points are variable-comparison and the open points are comparison-check+3. The dashed lines indicate midexposure times of individual echelle spectra.

(A color version of this figure is available in the online journal.)

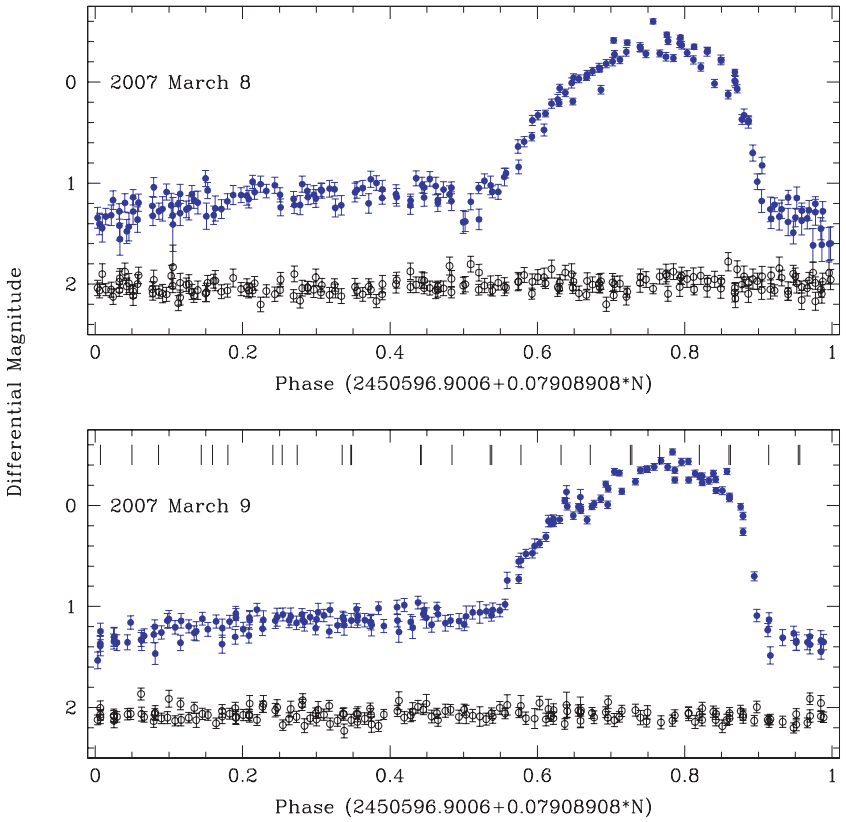

Figure 2. Orbital light curves of ST LMi during spectral observations. The dashed lines indicate midexposure times of individual echelle spectra. The filled points are variable-comparison and the open points are comparison-check+3.

(A color version of this figure is available in the online journal.)

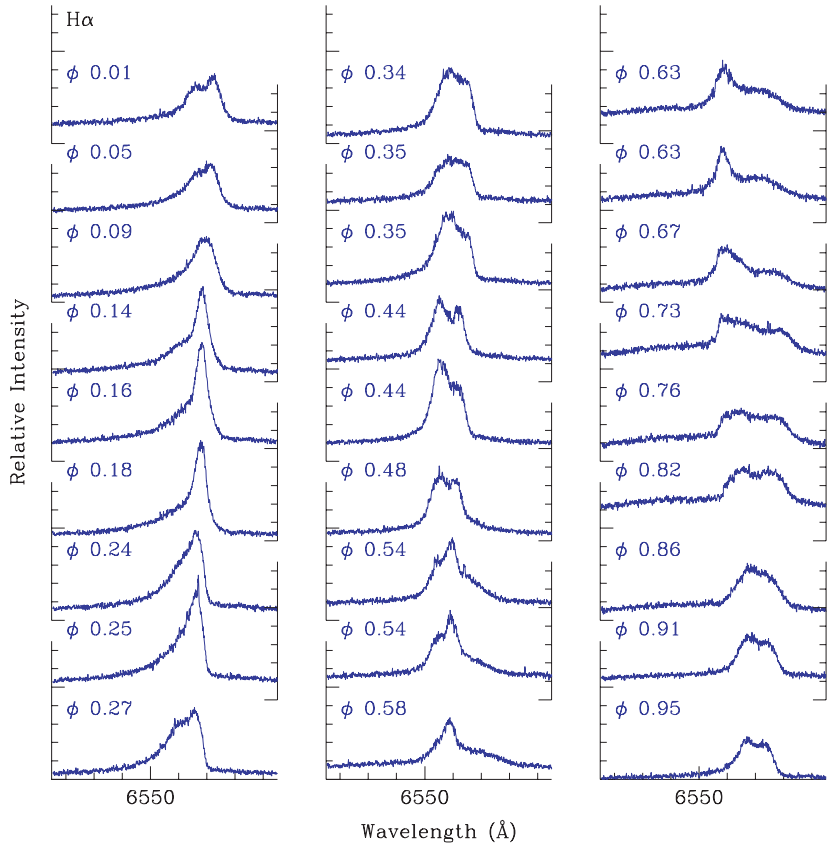

Figure 3. Hα spectral line during ST LMi high state sorted by orbital phase. Two spectra at redundant phases are not shown for clarity.
(A color version of this figure is available in the online journal.)

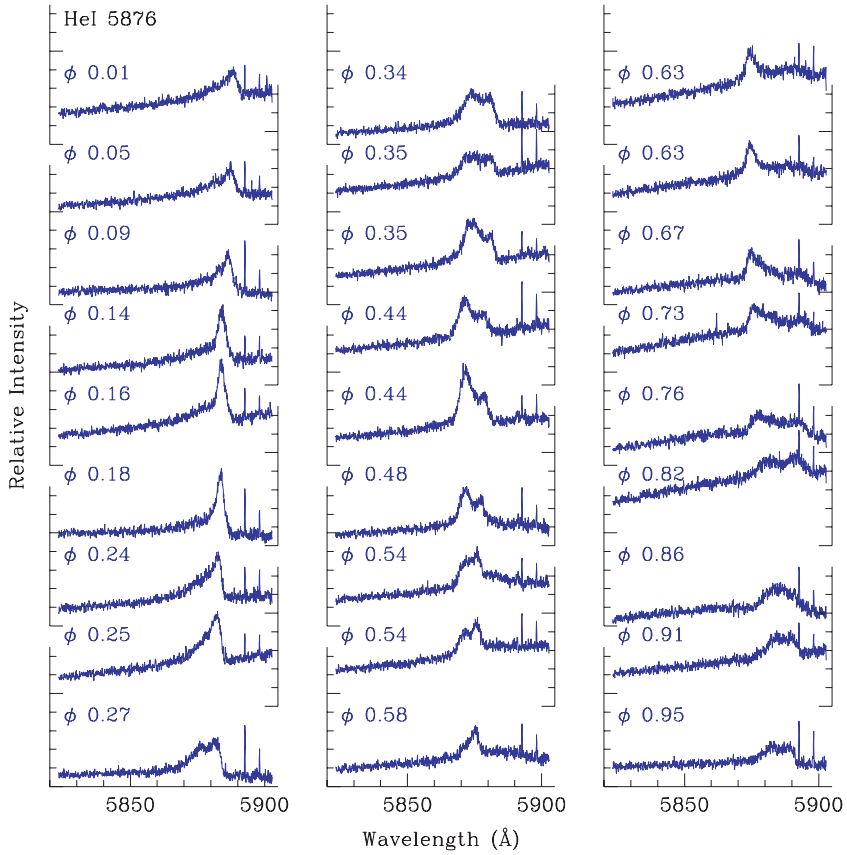

Figure 4. He I 5876 spectral line during ST LMi high state sorted by orbital phase. Na I $D_{1,2}$ night sky lines are also present.
(A color version of this figure is available in the online journal.)

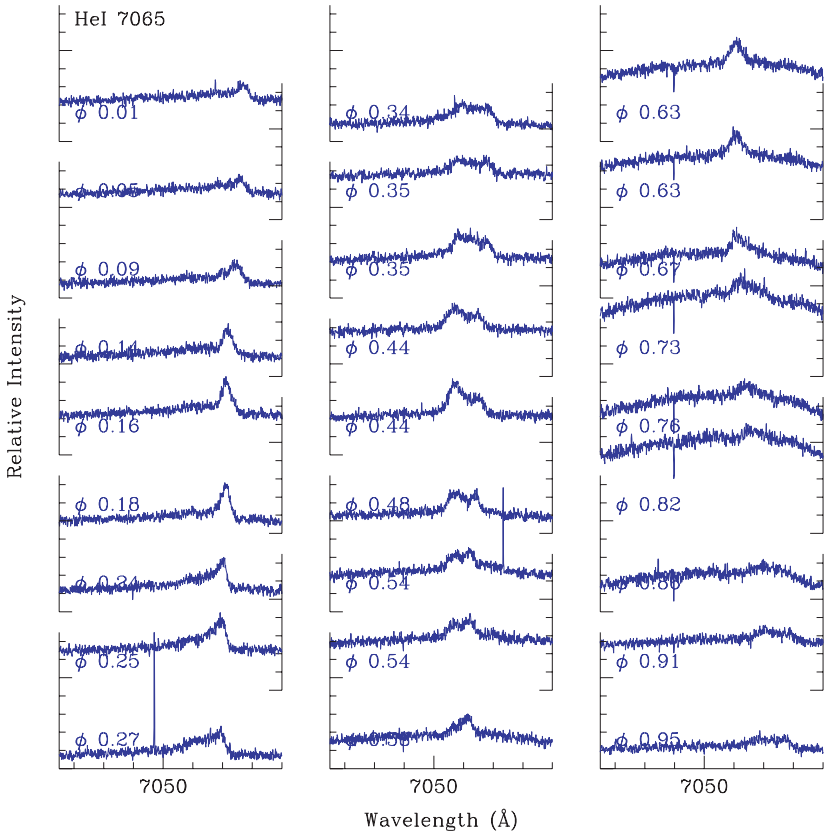

Figure 5. He I 7065 spectral line during ST LMi high state sorted by orbital phase. Orbital phasing is the same as for Figures 3 and 4.
(A color version of this figure is available in the online journal.)

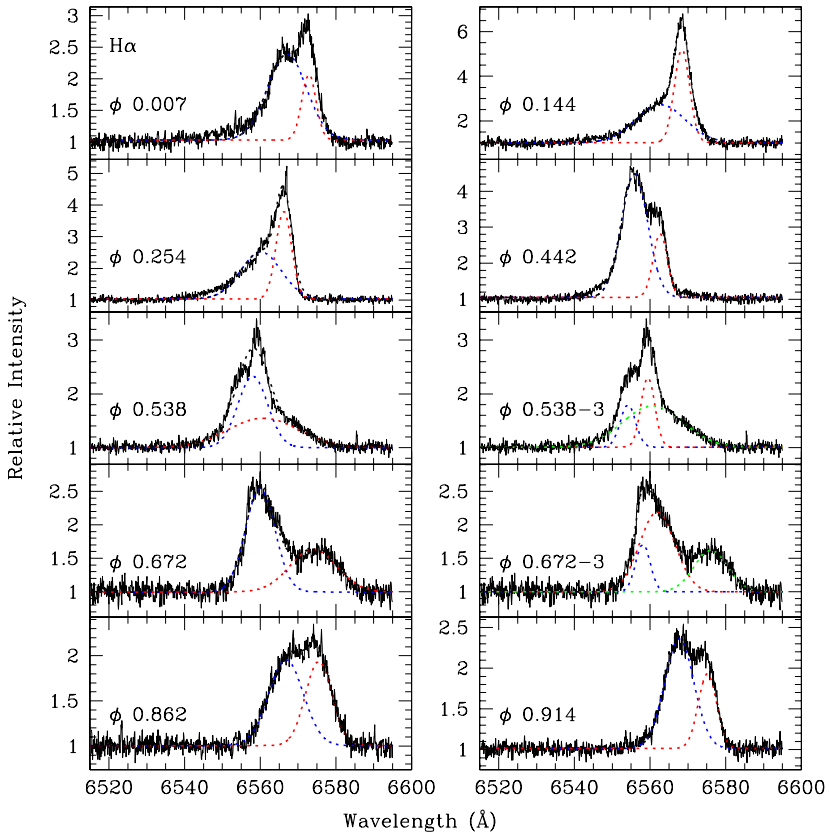

Figure 6. Hα spectral line at selected phases representing its changing profile over the orbit. The double Gaussian fits to the emission line profiles are shown. Phases 0.538 and 0.672 have a triple Gaussian fit added for comparison.
(A color version of this figure is available in the online journal.)

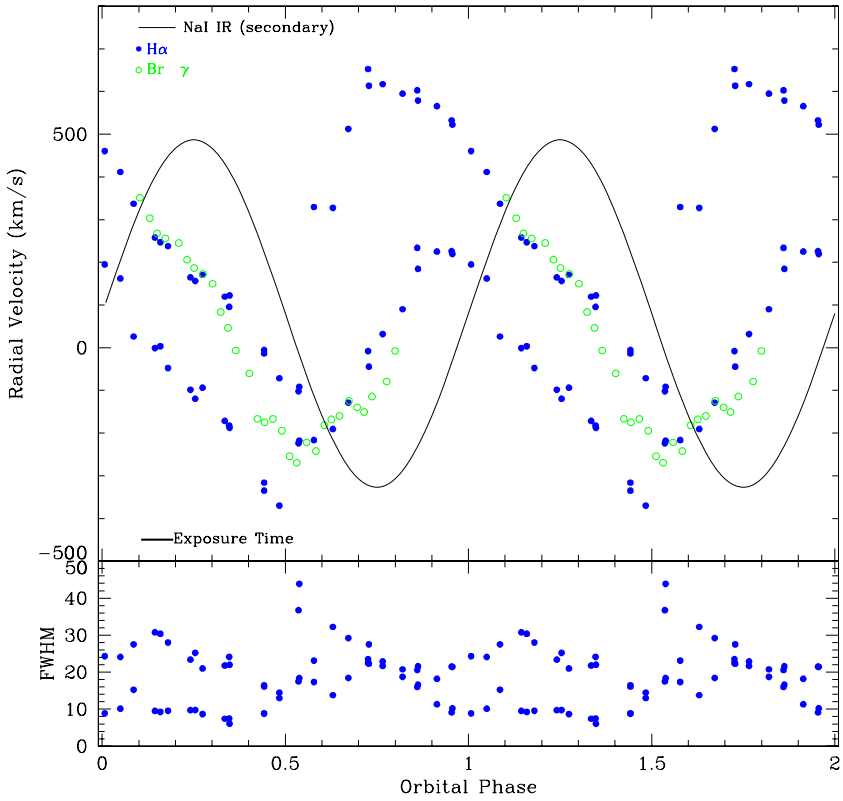

Figure 7. ST LMi RVs (top panel) of the peaks of the double Gaussian fits to Hα over the orbital phase. The filled dots are for Hα components A and B, the open dots for Brγ. The thick line at lower left in the top panel represents the length of the echelle exposure time in orbital phase units. The associated FWHMs for Hα components are in the bottom panel.

(A color version of this figure is available in the online journal.)

double Gaussian fits. When one recognizes the effect of these two methods, the differences in the RV curves make sense: in the phase interval 0.0–0.50 the centroid fit used in Paper I extracts the approximate average of the two parallel segments of the RV curves from the double Gaussian fit, while in the phase interval ~0.6–0.9, where the two components are well separated and identifiable, the "peak" method of Paper I as well as the double Gaussian show a high-velocity component reaching 600 km s^{-1} over the same phases (~0.6–0.9) as the orbital "hump" (see Figure 2). As an experiment, the line profiles from Paper I were fitted with double Gaussians using the same method as was employed for the 2007 echelle data. The resulting RV curves for the 2006 data were then indistinguishable, to within the errors, from the RVs plotted in Figure 8 of this paper. We note here that differences in the methods of extraction of RVs from the high-state line profiles in ST LMi are also likely to be responsible for the rather different interpretations of the origins of these lines more than 20 years ago (e.g., Stockman et al. 1983; Bailey et al. 1985); this is not a new difficulty with ST LMi. In the absence of a good understanding of the kinematic and spatial origins of the lines, it is difficult to know for sure what is the "best" method of RV extraction.

These difficulties are not confined to the determination of the RVs, but also extend to an ambiguity in the nature of the RV curves themselves. We assume here that the double Gaussian method provides the most useful RV characterization of the line profiles. These RVs are plotted in two panels of Figure 8, where they are coded according to two different assignments of the continuity with phase of the two emission line components. Adjacent data points have been connected by line segments to guide the eye. In the top panel, we see that two "parallel" sine-like curves with differing γ provide good continuity of the RVs with phase. However, such behavior is difficult to interpret physically unless a ring or rotating disk is involved, which seems very unlikely in a polar. In the bottom panel for the same data but different coding, we see that two crossing sine-like curves also provide a reasonable representation. Crossing curves have a plausible physical explanation as originating from two emission regions having different velocity vectors, each of which crosses γ velocity as system rotation brings each vector perpendicular to the line of sight.

In the absence of good models that might help distinguish these two representations, perhaps the data themselves offer clues. We note that the crossing RV curves in the bottom panel of Figure 8 each have rather strong discontinuities near phase 0.5, while the noncrossing RV curves in the top panel are smoothly continuous near phase 0.5. The behavior of FWHM near phase 0.5 can also be examined, as seen in the bottom panel of Figure 7. Once again, the choice of crossing sine curves leads to a sharp discontinuity of FWHM near phase 0.5, while the noncrossing representation is smoother. One would also like to examine equivalent widths (EWs) for discontinuities with phase, but our echelle spectra do not reliably measure the continuum. Integrated line flux might be used instead, but line flux for our echelle data is not trustworthy because of variable slit losses. So we are left with RV and FWHM, both of which "favor" a representation as two nearly parallel noncrossing RV curves, if discontinuities with phase are judged with disfavor.

However, we are not aware of any plausible kinematic explanation for two noncrossing RV curves in a polar; furthermore, discontinuities in RV, FWHM, and EW could be produced by

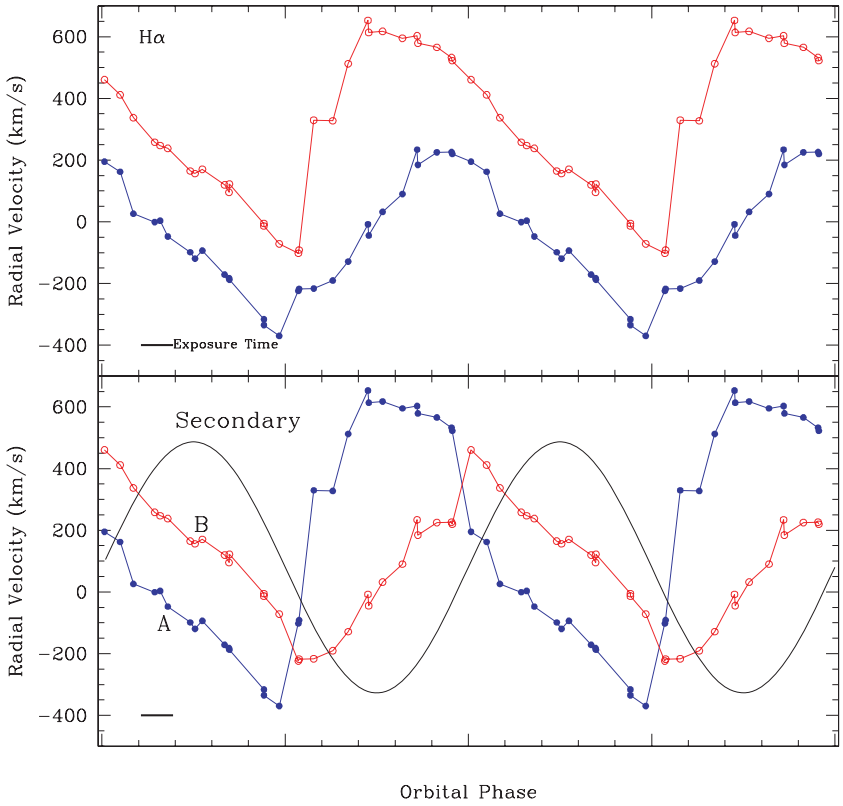

Figure 8. ST LMi RVs of the peaks of the double Gaussian fits to Hα over the orbital phase for two different interpretations representing crossover RVs (bottom panel) and noncrossover RVs (top panel). The sine curve is the RV solution for the secondary from the IR absorption lines in or near the photosphere (Howell et al. 2000). The thick line at lower left in the top panel represents the length of the echelle exposure time in orbital phase units.

(A color version of this figure is available in the online journal.)

"kinks" in whatever flows are responsible for the components of the emission line, a situation that might well occur as gas is threaded onto magnetic field lines and eventually flows along those lines. Although the smoothness of the parallel RV curves' representation is intriguing and deserving of discussion, in the remainder of this paper we will pursue only the representation consisting of two crossing RV curves. These are designated A and B in the bottom panel of Figure 8 (not to be confused with Bailey et al. 1985 components also labeled A and B). We will identify emission component A as the component that starts out at the shortest wavelength (blue wing) at phase 0.0 and identify the other emission component, B, as the one that starts out with the longest wavelength (red wing) at phase 0.0, remembering that phase 0.0 is inferior conjunction of the secondary star.

Most studies have concluded that ST LMi is a one-pole accretor (see Paper I for references). The broader emission line component A is moving strongly away from the observer at the time that the continuum light from the accretion spot on the WD is most directly facing the observer corresponding to the light curve "hump" seen in Figure 2. Therefore, component A almost certainly arises from some portion of the infall onto the main accreting pole.

Component B is generally attributed to either the secondary star or to some portion of the accretion stream near the secondary star (see Paper I for references). In Paper I the RVs from the centroid of the full line are in fact phased with the secondary star over most phases. However, in Figures 7 and 8 component B leads the secondary star's RV curve by ∼0.25 phase units, whereas the phase uncertainty in the secondary star's RV (solid line) is only ∼0.1 phase units. The RV curve of B is more sinusoidal than A and is, over most phases, the more narrow of the two components. Note that component B agrees well with the RV curve of the Brγ line in phase, amplitude, and shape (see Figure 8). We think that component B likely originates on the secondary's side of the center of mass. Using the model developed for a similar system, EF Eri (Howell et al. 2006) based on interconnected magnetic flux tubes between the two stars, similar to that observed and well studied in RS CVn systems, we believe that component B and the Brγ emission lines originate in a region between the two stars, probably where the magnetic fields of the two stars interact. Further evidence for such a picture is that during low states (Paper I) the RV curves of the weaker, narrower hydrogen emission lines (now lacking the broad component) match in phase and amplitude our component B and Brγ lines observed during a high state (Bailey et al. 1985). The presence of interconnected magnetic field lines from active regions on the secondary star to the WD appears to be a property that is independent of the mass transfer rate. We observe that the same emission features are present in the spectral lines in both high and low states. Therefore, the mass-transfer rate, whether on or off, is not having an observable effect on the structures that we feel are responsible for the emission line profiles.

Depending on the magnetic field strength of the WD, the orbital period, and the WD spin period, the structures that result from the accretion of ionized gas onto a magnetic WD can vary greatly, forming combinations of disks, streams, rings, and propellers (Norton et al. 2008). In a polar, the WD spin is synchronized with orbital motion, and the magnetic poles of the WD maintain a fixed orientation with respect to the secondary star as the system revolves. For polars having moderately dense flows and moderate magnetic field strengths, which is the situation for ST LMi in the high state, the flow is cooled

by a strong shock that mostly emits thermal X-rays, plus synchrotron radiation as the gas spirals around the magnetic field lines. Accreting gas follows a ballistic trajectory from the inner Lagrangian point to a point where the magnetic field pressure exceeds the ram pressure in the stream. Downstream from this coupling region, magnetic stresses inhibit the motion of plasma across the field lines, and the accreting gas flows along magnetic field lines to the magnetic pole(s), forming a standoff shock ∼10 radii above the WD (King 1993; Wynn & King 1995). The magnetic poles of the WD are, in general, not aligned with the secondary star, but are typically advanced prograde of the secondary, and tipped out of the plane. In the case of ST LMi, the prograde advance is ∼42° and the colatitude of the magnetic pole is ∼141°. This means that downstream from the coupling region the flow is no longer confined to the orbital plane and 3D modeling must be employed.

The gas streams and funnels in polars are complex and detailed modeling is difficult because the motion is a nonlinear 3D hydromagnetic flow (e.g., Ferrario & Wehrse 1999; Norton et al. 2004). However, the optically thin portions of the flow produce emission lines whose observed RVs can, in many cases, be used to determine the locations, orientations, and motions of the various components of the accretion structures. Using RV curves, synthetic trailed spectra, and Doppler tomagraphic maps, investigators have identified a number of features that appear in various combinations in particular polars (e.g., Schwope et al. 1997 (HU Aqr, high state); Schwope et al. 2000 (QQ Vul); Schwarz et al. 2002 (AM Her); Schwarz et al. 2005 (BY Cam)). These features include (1) a quasi-chromosphere at the irradiated inner hemisphere of the secondary star, which may be asymetrical due to shadowing by the steam, (2) emission from the ballistic stream leaving L1 which is often wider than predicted, (3) the coupling region where increased dissipation is expected to occur as the stream is forced to leave the orbital plane, and (4) the magnetically controlled stream leading to the magnetic pole. These are the kinds of features that may be present in our ST LMi spectra and could reproduce the complex line profiles.

We thank the Kitt Peak Director, Buell Januzzi, and Mike Merrill for their allocation of 4 m time for this pilot project. We also thank Daryl Willmarth for help with our instrument setup.

REFERENCES

Bailey, J., et al. 1985, MNRAS, 215, 179
Cropper, M. 1986, MNRAS, 222, 853
Ferrario, L., Bailey, J., & Wickramasinghe, D. T. 1993, MNRAS, 262, 285
Ferrario, L., & Wehrse, R. 1999, MNRAS, 310, 189
Groth, E. J. 1986, AJ, 91, 1244
Hellier, C. 2001, Cataclysmic Variable Stars (Chichester: Springer-Praxis)
Henden, A. A., & Honeycutt, R. K. 1997, PASP, 109, 441
Honeycutt, R. K. 1992, PASP, 104, 435
Howell, S. B., Ciardi, D. R., Dhillon, V. S., & Skidmore, W. 2000, ApJ, 520, 904
Howell, S. B., Walter, F. M., Harrison, T. E., Huber, M. E., Becker, R. H., & White, R. L. 2006, ApJ, 652, 709
Hroch, F. 1998, in Proc. 29th Conf. on Variable Star Research, Computer Programs for CCD Photometry, ed. J. Dusek & M. Zejda (Brno: Masaryk Univ.), 30
Kafka, S., Howell, S. B., Honeycutt, R. K., & Robertson, J. W. 2007, AJ, 133, 1645
King, A. R. 1993, MNRAS, 261, 144
Norton, A. J., Butters, O. W., Parker, T. L., & Wynn, G. A. 2008, ApJ, 672, 524
Norton, A. J., Wynn, G. A., & Somerscales, R. V. 2004, ApJ, 614, 349
Peacock, T., Cropper, M., Bailey, J., Hough, J. H., & Wickramasinghe, D. T. 1992, MNRAS, 259, 583
Potter, S. B. 2000, MNRAS, 314, 672
Schwarz, R., Hedelt, P., Rau, A., Staude, A., & Schwope, A. D. 2002, in ASP Conf. Ser. 261, The Physics of Cataclysmic Variables and Related Objects, ed. B. T. Gänsick, K. Beuermann, & K. Reinsch (San Francisco, CA: ASP), 167
Schwarz, R., Schwope, A. D., Staude, A., & Remillard, R. A. 2005, A&A, 444, 213
Schwope, A. D., Catalán, M. S., Beuermann, K., Metzner, A., Smith, R. C., & Steeghs, D. 2000, MNRAS, 313, 533
Schwope, A. D., Mantel, K.-H., & Horne, K. 1997, A&A, 319, 894
Stetson, P. 1987, PASP, 99, 191
Stockman, H. S., Foltz, C. B., Schmidt, G. D., & Tapia, S. 1983, ApJ, 271, 725
Stockman, H. S., & Schmidt, G. D. 1996, ApJ, 486, 883
Warner, B. 1995, Cataclysmic Variable Stars (Cambridge: Cambridge Univ. Press)
Wynn, G. A., & King, A. R. 1995, MNRAS, 275, 9